Sustainable Cities and Society 98 (2023) 104833

Contents lists available at ScienceDirect

Sustainable Cities and Society

journal homepage: www.elsevier.com/locate/scs

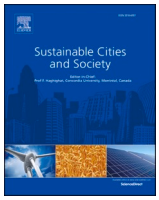

Monitoring diurnal dynamics of surface urban heat island for urban agglomerations using ECOSTRESS land surface temperature observations

Yue Chang [a,b], Jingfeng Xiao [c], Xuxiang Li [d], Qihao Weng [a,b,*]

[a] JC STEM Lab of Earth Observations, Department of Land Surveying and Geo-Informatics, The Hong Kong Polytechnic University, Hung Hom, Hong Kong
[b] Research Centre for Artificial Intelligence in Geomatics, The Hong Kong Polytechnic University, Hung Hom, Hong Kong
[c] Earth Systems Research Center, Institute for the Study of Earth, Oceans, and Space, University of New Hampshire, Durham, NH 03820, USA
[d] Institute of Global Environmental Change, Xi'an Jiaotong University, Xi'an, Shaanxi Province 710049, China

ARTICLE INFO

Keywords:
International space station
Urbanization
Urban agglomerations
ECOSTRESS
Thermal remote sensing
Diurnal SUHI dynamics

ABSTRACT

Extreme heat exposure at the regional scale is warranted for special attention due to the changing global climate yet notable regional disparities in the effect of warming. NASA's latest ECOSTRESS mission generates LST images with a swath width of about 400 km and a 70-m resolution for varying times of day/night and provides a new opportunity for regional SUHI studies. Here we demonstrated the capability of ECOSTRESS data for studying spatiotemporal variations of LST and SUHI over an urban agglomeration that centers on a megacity, Xi'an, in Northwest China and includes cities of various sizes and geographical and economic settings. Our results revealed the unequal exposures of different-sized cities to SUHI effects in the diurnal cycle, with a maximum value of about 10 °C. Meanwhile, inter-city SUHI showed higher spatial variability in the late morning, midday, and early afternoon than in the evening, midnight, and early morning. Urban vegetation and percent imperviousness can regulate SUHI spatial variations in each city, and the impact varied across cities or at different diurnal times. The findings can have implications for assessing extreme heat exposure in regional cities, enlightening the urban SUHI mitigation strategies, and informing future regional sustainability.

1. Introduction

Urbanization dramatically modifies the Earth's surface and transforms natural land covers into urban landscapes (Rigden & Li, 2017; Zheng et al., 2021). Such changes can lead to a series of environmental issues, a well-documented of which is urban heat island (UHI), the phenomenon that temperature in the urban area is generally higher than that in its surrounding area (Voogt & Oke, 2003). Excessive heat in urban areas can increase energy and water consumption, aggravate air pollution, exacerbate health hazards especially during heat waves, affect public living comfort, and degrade ecosystem functions (Hu et al., 2020; Yang et al., 2020). Furthermore, these adverse impacts are expected to be aggravated in the foreseeable warmer future without effective heat adaptation strategies (Mentaschi et al., 2022). Therefore, exploring the UHI phenomenon and its underlying mechanisms can inform urban heat mitigation strategies and has received increasing attention.

UHI is characterized by not only high temporal variability but also strong spatial heterogeneity (Krayenhoff et al., 2018; Liu et al., 2022). Temperature data availability is of primary importance for UHI studies, and further determines the UHI types, which mainly include air temperature (AT) based canopy layer urban heat island (CUHI) and land surface temperature (LST) based surface urban heat island (SUHI) (Voogt & Oke, 2003). Benefiting from continuously high-frequency AT records, the temporal variability of CUHI has been well studied at multiple time scales in the literature (Kim & Brown, 2021; Siddiqui et al., 2021). However, it is also evident that both observational and model-estimated AT data are generally not suitable for the detailed spatial analysis of CUHI due to the limited number of meteorological stations across urban areas. By contrast, LST derived from satellites has the capability to assess the spatial variability of SUHI at different space/time scales owing to the spatially continuous and regular observations as well as the broad spatial coverage (Zhou et al., 2019; Zhu et al., 2019). Constrained by the low temporal resolution of conventional urban remote sensing systems, most efforts related to the SUHI have been focused on a limited number of fixed time-nodes within the course of the diurnal cycle at diverse time scales (e.g., seasonal and inter-annual scales). Moreover, to overcome the deficiency of these observational LST data, some studies have developed different methods

* Corresponding author.
E-mail address: qihao.weng@polyu.edu.hk (Q. Weng).

https://doi.org/10.1016/j.scs.2023.104833
Received 4 May 2023; Received in revised form 27 July 2023; Accepted 27 July 2023
Available online 30 July 2023

(e.g., temporal interpolation and spatial downscaling techniques) to characterize the SUHI patterns at fine spatial-temporal scales (Lai et al., 2018; Weng et al., 2014). However, such approaches have limitations due to inherent model assumptions and may introduce substantial uncertainties when coping with missing LST data, especially over a large-scale region including diverse urban environments. Consequently, more optimal schemes are required to formulate a more reliable and accurate understanding of SUHI diurnal dynamics at varying spatial scales.

An urban agglomeration is formed by a group of cities that have not only a compact spatial organization but also tight economic relations (Batten, 1995; Zhou et al., 2018). With economic development and population aggregation, urban agglomeration becomes a common spatial form of regional urbanization, which exacerbates the regional SUHI risk (Fang & Yu, 2017; Fu et al., 2022). Accordingly, SUHI over urban agglomerations arouses widespread attention in recent years. Owing to the moderate spatial resolution and long-term records, LST derived from polar-orbiting satellites (e.g., Landsat series, Terra, Aqua) is most extensively applied to the SUHI studies of urban agglomerations (Feng et al., 2021; Wang et al., 2022; Yu et al., 2019). While certainly insightful, the following limitations remain in elaborating SUHI effects over urban agglomerations. First, most current studies are still intent on the SUHI patterns in individual cities or among some popular cities across the globe or a country, and only a few studies provide insight into urban agglomerations at a regional scale (Geng et al., 2021; Peng et al., 2022; Zhou et al., 2019). Second, previous studies mainly evaluated the SUHI effects of mega-cities and large cities (i.e., city-administrated districts) in urban agglomerations, while ignoring the analysis of small cities (i.e., county-administrated districts), whose urban extent may be only tens of or several square kilometers or even less. As the fundamental unit of regional planning and economic development, county-administrated districts may play an important role in implementing SUHI mitigation strategies for the improvement of the regional thermal environment. Additionally, low income, inadequate green infrastructure and ongoing urbanization may make residents more susceptible to extreme heat. Thus, SUHI risk assessment in small cities requires more attention. Third, analysis of regional SUHI diurnal dynamics at a fine spatial scale is hindered by the lack of available LST data with both large swath and high spatiotemporal resolution. Therefore, knowledge on meticulous patterns of SUHI variations in urban agglomerations during a diurnal cycle is largely restricted.

The knowledge gaps on SUHI diurnal cycle in urban agglomerations can now potentially be narrowed down with LST data acquired by NASA's latest spaceborne thermal radiometer (i.e., ECOSTRESS). ECOSTRESS instrument was deployed on the International Space Station (ISS) on July 3, 2018, and includes five spectral channels from 8 to 12.5 μm for accurately measuring LST data (Hulley et al., 2021). With the special orbit of ISS, ECOSTRESS has the diurnal sampling ability to collect LST measurements at a high temporal resolution of 1 to 5 days and spatial resolution of 70 m (Xiao et al., 2021). The ECOSTRESS LST data have been used to reveal the vulnerability of cities to heat waves at the fine scale (Hulley et al., 2019) and diurnal variations of the thermal environment among urban local climate zones in a megacity (Chang et al., 2021). Besides, compared to the Landsat and ASTER imagery with similar spatial resolution, a remarkable advantage of ECOSTRESS data is its much larger swath width of about 400 km, which can provide the simultaneous LST record of different cities in an urban agglomeration. Since the impacts of SUHI on health and energy consumption vary diurnally, ECOSTRESS LST data with these unique advantages together may have the potential to generate new insights into such assessments instead of the temporally or spatially averaged results in previous studies. Meanwhile, ECOSTRESS LST data are also more likely to capture the real heat threat during extreme weather events, as such issues (e.g., heat waves) are generally frequent but only last a few days. Considering the reasons above, ECOSTRESS can offer an unprecedented opportunity to advance our understanding of the SUHI diurnal dynamics in urban agglomerations.

Understanding the underlying mechanism of SUHI is crucial for developing targeted heat mitigation strategies to minimize the adverse consequences of heat waves, thereby enhancing urban resilience and promoting sustainable urban development. The driving factors of SUHI have been extensively studied in the literature, with key factors including land cover, meteorological conditions, anthropogenic heat emissions and urban morphology (Geng et al., 2021; Hu et al., 2020; Zhou et al., 2019). Many studies have demonstrated that green space and vegetation in cities play an important role in alleviating SUHI via reducing the amount of solar radiation absorbed by urban surface and increasing evapotranspiration (Feng et al., 2021; Ossola et al., 2021; Weng et al., 2011). Conversely, impervious surface and anthropogenic heat emissions are generally identified as significant contributors to the intensification of SUHI (Du et al., 2016; Liu et al., 2022; Yu et al., 2019). Urban morphology, encompassing size, compactness, fractal dimension and landscape patches, are also considered to have impacts on the spatial variability of SUHI within a city or among cities (Fu et al., 2022; Hou et al., 2023). Furthermore, the intricate interaction between these factors and local meteorological conditions amplifies the complexity of SUHI dynamics especially at regional or larger spatial scales (Peng et al., 2012; Sun et al., 2019; Zhou et al., 2018). Therefore, more efforts are still required to unravel the potential effect of these driving factors on SUHI at different spatial and temporal scales.

In this study, we demonstrated the capability of ECOSTRESS LST data for analyzing SUHI diurnal dynamics in an urban agglomeration that spans broad regions and includes cities of various sizes. Specifically, we explored SUHI diurnal patterns and the possible determinants over cities in the Guanzhong Urban Agglomeration (GUA) of Shaanxi Province, Northwest China using ECOSTRESS LST data acquired during the four warm months (June through September) from 2019 to 2022. The aims of this study were: 1) to compare the capabilities of ECOSTRESS, Landsat, ASTER, and MODIS LST data in acquiring LST measurements suitable for studying the urban agglomeration; 2) to characterize the inter- and intra-city SUHI variability at varying times in the diurnal cycle over GUA; and 3) to analyze how relationships between SUHI and the possible drivers vary diurnally at city and pixel scales. Our study provides a more complete picture of SUHI patterns at the urban agglomeration level at higher spatial (i.e., encompassed a wide range of city size and a variety of urban environments) and temporal (i.e., included more time points in the diurnal cycle) scales. As the findings of the study focused on administration units, they can inform practicable heat mitigation measures locally and support future regional sustainable development.

2. Data and methods

2.1. Study area

We selected the Guanzhong region, located in central Shaanxi Province of western China, as the study area. The topography of this region is dominated by flat plains, with the Qinling Mountains in the south and the Loess Plateau in the north. Thus, most cities are concentrated in the central plain, and a few cities are scattered across mountainous areas (Fig. 1). The Guanzhong Urban Agglomeration (GUA) refers to all the cities in this region, consisting of one mega-city (Xi'an), four large cities (Baoji, Xianyang, Tongchuan and Weinan), and 38 small cities (counties) (Yang et al., 2022). GUA is the greatest urban agglomeration in northwestern China. It has a total area of ~55,297 km^2 and spans ~220 km from north to south and ~370 km in the east-west direction. Meanwhile, the population size of GUA was 24.6 million in 2019. Among cities in GUA, the mega-city Xi'an has a population of 10.2 million, which is about 1/3 of the total population of Shaanxi province (Yang et al., 2022). Situated on the boundary between a humid subtropical (Cwa) and semi-arid (BSk) climate under the Köppen climate classification (Peel et al., 2007), this region has hot, humid summers and

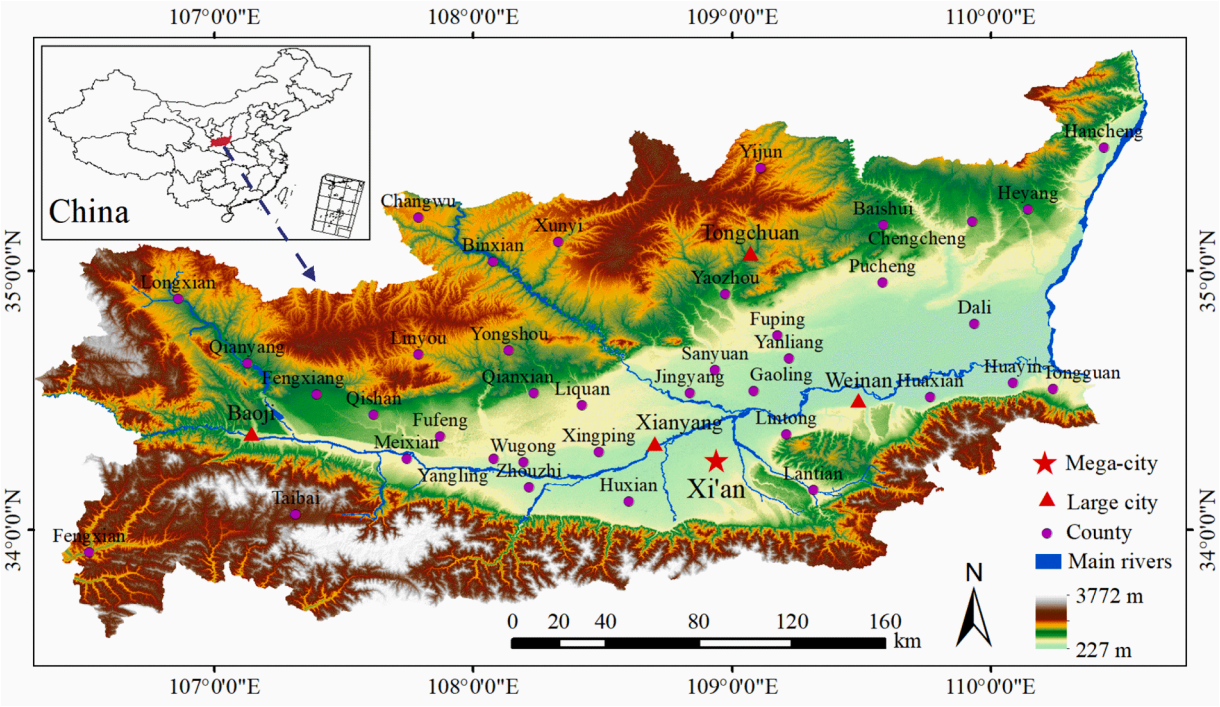

Fig. 1. The location of the study area, the Guanzhong Urban Agglomeration (GUA), Shaanxi Province, China, and the spatial distribution of 43 cities (one megacity, four large cities, and 38 small cities).

cold, dry winters, with average seasonal temperature of 24.9 °C and 1.5 °C, respectively, according to the 2020 Shaanxi Statistical Yearbook. The GUA has been experiencing rapid urban growth with the implementation of China's Western Development Strategy since 2000. Continuous urbanization associated with the aggregation of population and urban expansion has severely deteriorated the regional thermal environment, but SUHI here was rarely investigated since most previous SUHI studies were focused on the developed regions. Thus, there is an imperative demand to assess the SUHI risk over GUA to help better confront the warming future. Another important reason for selecting GUA is that it includes a wide range of urban sizes from several to hundreds of square kilometers, which can allow a solid evaluation of the capability of ECOSTRESS LST for capturing the fine-grained spatial variability of SUHI over diverse urban environments in urban agglomerations. In addition, through the research on GUA, we aim to call for greater attention to developing regions, where experience rapid urbanization and the local population may be more sensitive and vulnerable to the SUHI risk.

2.2. ECOSTRESS LST data

The ECOSTRESS mission, which is managed by NASA's Jet Propulsion Laboratory, provides 4 different levels of data products that incorporate additional auxiliary information as the level increases. ECOSTRESS LST data were obtained from the ECOSTRESS Level-2 science product (ECO2LSTE), which can be downloaded from the website of https://lpdaac.usgs.gov/. The ECO2LSTE including LST and emissivity data is retrieved by the Temperature Emissivity Separation (TES) method (Hook et al., 2020). To further improve the accuracy and stability of LST retrieval, this algorithm is integrated with an enhanced Water Vapor Scaling (WVS) atmospheric correction scheme. ECOSTRESS LST has a 70 m × 70 m spatial resolution, which is resampled from the original pixel size of 38 m × 68 m (Xiao et al., 2021). The ECOSTRESS LST product is of high quality and has good agreement with ground-based LST records at all global validation sites (overall root mean square error = 1.07 K, $r^2 > 0.988$, and mean absolute error = 0.4 K) (Hulley et al., 2021). Another validation effort conducted by Hook et al. (2020) reported uncertainties for the product at <1 K. In this study, we focused the analysis of SUHI diurnal dynamics on the warm months (June through September) in GUA. This period was selected due to the high frequency of extreme heat, which has significant impacts on urban populations. All available ECOSTRESS LST imagery in these four months from 2019 to 2022, as well as the corresponding cloud mask and quality control layers, were collected for subsequent data processing. Then, we removed the LST imagery which covered only a small portion of the study area or in which extensive quality issue (i.e., cloud contamination) was identified. Afterwards, we filtered these data to reserve images that had cloud-free LST records for most urban areas of GUA. Considering that inter-urban SUHI is the primary target of this study, we tended to retain the images including more available measurements in urban areas although they may not possess a large percentage of cloud-free pixels across the whole region. Finally, twelve ECOSTRESS LST scenes acquired at different times in the diurnal cycle were used for further analysis. Detailed information on the observation times of these LST images was presented in Appendix Table A.1. Note that all times used in this study were converted to local time (UTC + 8) and shown as a 24-hour clock.

2.3. Ancillary data

Besides ECOSTRESS LST data, we also employed LST data from Landsat TIRS, ASTER, and MODIS to assess their differentiation in characterizing SUHI variability across urban agglomerations. Landsat imagery was downloaded from the EarthExplorer website (https://earthexplorer.usgs.gov). The Landsat-8 LST data has a native spatial resolution of 100 m and a temporal resolution of about 16 days. ASTER LST (AST08) data were obtained from NASA's Earthdata (https://earthdata.nasa.gov/). ASTER onboard the Terra satellite includes five thermal infrared (TIR) channels for generating LST product globally. The ASTER LST has a similar temporal resolution to Landsat-8 LST but has a slightly higher spatial resolution of 90 m. Owing to high accuracy and fine spatial resolution, these two LST datasets have been widely applied to

urban environmental studies. In this study, we collected available Landsat (path/row: 126–128/36–37) and ASTER LST imagery from June 1, 2020, to September 30, 2020 of the study area. The daily MODIS LST product was obtained from NASA's Atmosphere Archive and Distribution System website (https://ladsweb.modaps.eosdis.nasa.gov/). MODIS LST data is generated from two MODIS TIR bands by the generalized split-window algorithm (Wan, 2008) and is available at a 1-km resolution. According to the overpass dates of the twelve ECOSTRESS LST scenes, three MODIS LST images including one MOD11A1 image and two MYD11A1 images were finally used in this study. Each selected MODIS LST image has the same acquisition date and close observation time as the corresponding ECOSTRESS LST scene. The two MYD11A1 images were acquired on July 26, 2020 (13:06) and August 1, 2021 (12:42), while the acquisition time of the MOD11A1 image was 10:30 on August 6, 2022.

The land cover map of GUA was acquired from the Chinese Academy of Sciences (CAS)'s Resource and Environment Science and Data Center (RESDC) (http://www.resdc.cn/). This 30 m-resolution land cover map was mainly generated from Landsat-8 images and includes 25 land cover types (Liu et al., 2005). The 25 types can be combined into six broad categories: bare land, forest land, grassland, water body and developed land (including urban land, rural settlements, and others beyond cities such as roads, large industrial and mining areas, and airports). This dataset was generated via human-computer interaction based on geographic knowledge and then improved by other ancillary data (e.g., GF-2, UAV aerial images), field trips, and expert knowledge (Zhang et al., 2014). Compared to six existing mainstream datasets, this dataset has higher accuracy in urban-boundary detection and has an overall accuracy of over 90% (Kuang et al., 2021). In this study, the land cover map of 2020 was used to determine the urban and rural areas for cities in GUA.

Surface elevation data were downloaded from the Geospatial Data Cloud website (http://www.gscloud.cn). This data was retrieved from the ASTER GDEM V2 product and has a 30-m resolution. We utilized this dataset to depict the distribution of elevation across the study area and to assist in the delineation of the urban and rural areas.

Background climate variables including solar radiation, wind speed, precipitation and air temperature were retrieved from WorldClim 2.1 (https://www.worldclim.org/). This dataset provides aggregated monthly climate data for the period from 1970 to 2000 with a high spatial resolution of 1 km (Fick & Hijmans, 2017). In this study, we used the summertime imagery in this dataset to analyze the impact of background climate on SUHI variability among cities (Guo et al., 2020; Zhou et al., 2018). Although the climate variables may have changed during the study period, the use of the 1970–2000 period as background climate data can provide a widely accepted and comprehensive dataset for correlation analysis, especially considering the relatively stable nature of the background climate (Peng et al., 2012; Peng et al., 2019; Yao et al., 2023).

The Normalized Difference Vegetation Index (NDVI) data were obtained through the National Ecosystem Science Data Center (http://www.nesdc.org.cn), a public information-sharing platform from the National Science and Technology Infrastructure of China. This dataset was developed by using all Landsat imagery for each year via Google Earth Engine (Yang et al., 2019) and can provide annual maximum NDVI images with a spatial resolution of 30 m in China from 2000 to 2020 (https://doi.org/10.12199/nesdc.ecodb.rs.2021.012). The NDVI data for 2020 was employed to examine the cooling effect of vegetation in this study.

We also used impervious surface percentage (ISP) data that were generated by Kuang et al. (2021). This dataset includes the fractions of impervious surface area and green space at 30-m resolution for cities in China over the period from 2000 to 2018. Specifically, the urban boundaries used in this dataset were identified by the land cover map from the RESDC. Validation results showed that it was consistent with six other urban land datasets with a correlation coefficient of 0.91 and a root mean square error of 0.10 (Kuang et al., 2021). Because of the data availability, we used the ISP data of 2018 to identify the difference in imperviousness of urban areas across GUA.

The population distribution map was retrieved from the LandScan Global product developed by the Oak Ridge National Laboratory, which can be downloaded from the website of https://landscan.ornl.gov/. LandScan products provide the global ambient population distribution data at 1-km resolution for the years from 2000 to 2021 (Sims et al., 2022). In this study, we used LandScan Global 2020 to evaluate the population density in GUA. In addition, GDP data acquired from the 2020 Shaanxi Statistical Yearbook was used as a metric to indicate socioeconomic variations among the cities in the study area. A concise summary of the basic information of the data utilized in this study can be found in Appendix Table A.2.

2.4. Comparison of ECOSTRESS LST with LANDSAT, ASTER, and MODIS LST

The framework of this study is presented in Fig. 2. We first implemented a compendious comparison between ECOSTRESS and Landsat, ASTER and MODIS to generalize their differences in characterizing LST across urban agglomerations. We chose these three LST products for comparison because they were the main data sources (> 85%) for SUHI studies (Weng, 2009; Weng et al., 2011; Zhou et al., 2019). Since the accuracy of these LST data has been extensively validated (Hook et al., 2020; Hook et al., 2007), our analysis focused on their contrasts in terms of spatial coverage per image, temporal resolution, and spatial resolution. We collected all LST scenes of the four satellites/sensors for the time span from June 1, 2020, to September 30, 2020. To facilitate the comparison, the commonly used products were classified into two groups via the spatial resolution, including Landsat and ASTER LST (Group 1), and MODIS LST (Group 2). For Group 1 with a similar spatial resolution to ECOSTRESS LST, we initially compared their performance in generating available LST measurements for the GUA. In this step, we extracted the spatial extent of high-quality Landsat and ASTER imagery (cloud cover of less than 10% for each image) and compared their coverage with that of an ECOSTRESS image. Then we evaluated their potential in providing high temporal resolution data by creating three sampling areas throughout the GUA. In this step, all the images covering the sampling areas including those with cloud contamination were recorded. For Group 2 with daily sampling and large spatial extent (1200 km × 1200 km), we mainly examined their ability in capturing the spatial variability of LST for cities of different sizes across urban agglomerations. We chose three cities (i.e., Fengxian, Dali and Baoji) with a large span of urban sizes to exemplify the difference between MODIS and ECOSTRESS LST. These cities were composed of two county-administrated districts and one city-administrated district in GUA, with varying urban sizes of 0.53, 11.81, and 25.45 km^2, respectively. Then three pairs of ECOSTRESS and MODIS measurements acquired within short time intervals were employed to characterize LST for these cities. We visually evaluated each image to determine if the heat signature from urban areas was discernible from the background and extracted LST values for all pixels in urban areas of the three cities to examine the ability of ECOSTRESS and MODIS data in measuring spatial LST variability.

2.5. Exploring SUHI diurnal patterns in GUA and the possible determinants

We then quantified SUHI characteristics among cities of GUA at varying times in the diurnal cycle using these twelve ECOSTRESS LST scenes from 2019 to 2022. In this study, the simplified urban-extent algorithm was employed to identify urban and rural areas in each city for SUHI intensity calculation (Chakraborty & Lee, 2019; Chakraborty et al., 2020). This approach was developed to administratively characterize inter- and intra-city SUHI variability to facilitate local

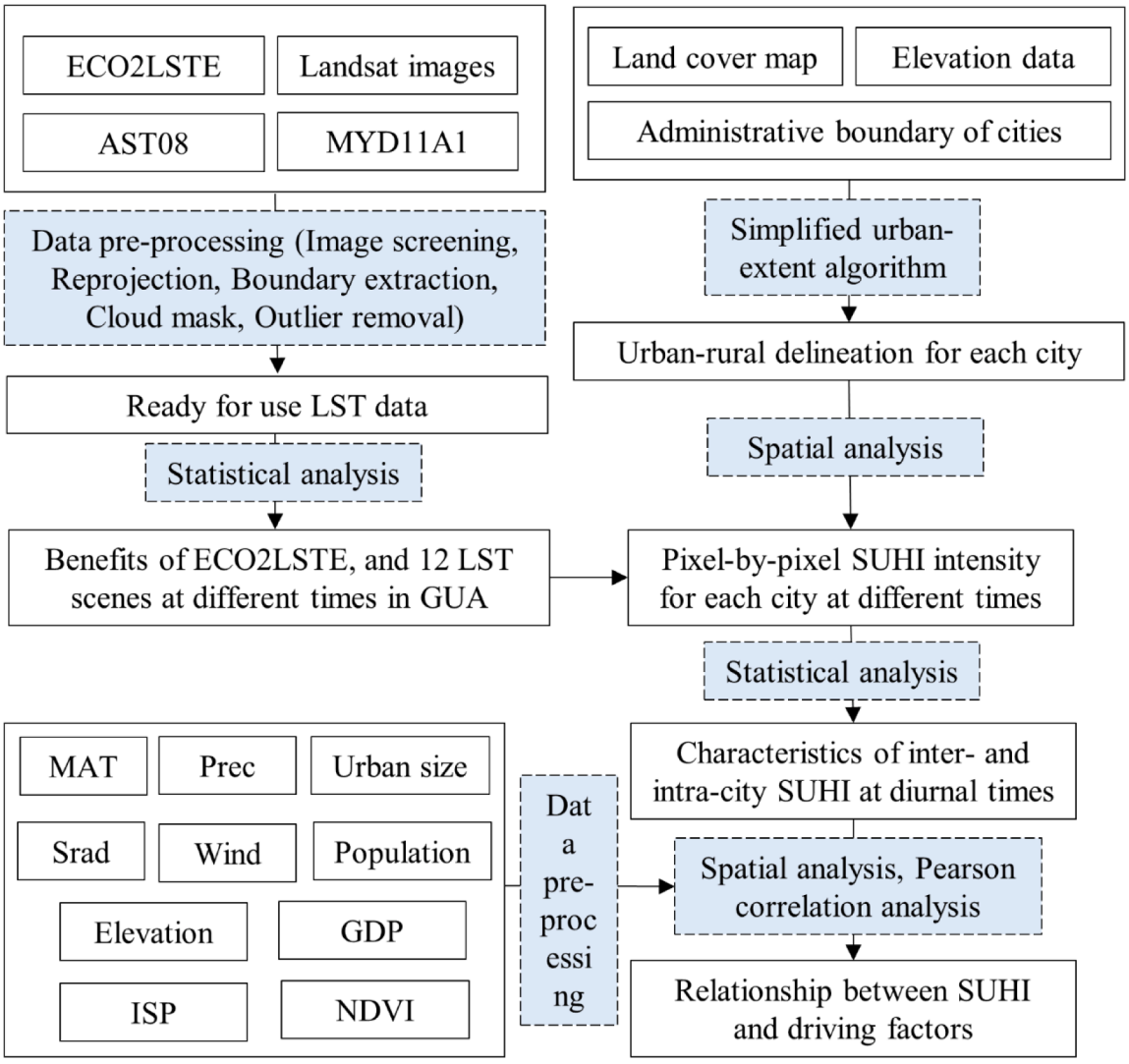

Fig. 2. Flowchart of this study. The software packages employed for data analysis and visualization in this study include ArcGIS, Python, and Origin.

policy-making. The land cover map of 2020, elevation data and administrative extent of each city were used for urban-rural delineations in GUA through the following steps. First, to reduce the elevation impacts, we filtered out pixels with elevation 50 m higher or lower than the median of the elevation of all urban pixels for each city (Liu et al., 2022). Second, all pixels with the label of "urban land" within the administrative extent of each city were classified as urban areas, while all the other pixels (with those classified as water body, other built-up areas, permanent wetland, snow, and ice excluded) were grouped as the referenced rural areas. Third, for cities in mountainous areas, which are characterized by high urban elevation (over 700 m), small urban size (several square kilometers or even less) and distribution along mountain valleys, we retained pixels within a 5 km buffer zone of the urban center as the rural areas to diminish the influence of undulating mountains. The urban-rural delineations for each city in the study area are illustrated in Fig. 3. Concurrently, we applied the corresponding cloud mask files to remove cloud pixels from the ECOSTRESS scenes. It is noteworthy that cloud-containing pixels may not be completely filtered out across the whole region during the data processing since certain clouds especially those in the alpine areas can be difficult to identify (Gustine et al., 2022). Therefore, only cities in which urban and rural areas both had over 90% available ECOSTRESS LST pixels were included for the subsequent SUHI analysis to further reduce the influence of the cloud. For each city, we quantified the pixel-by-pixel SUHI intensity in the urban areas using averaged LST value of all pixels in the rural areas as a reference, with the following equation (Voogt & Oke, 2003):

$$\Delta T_{urban,pixel} = T_{urban,pixel} - T_{rural} \quad (1)$$

where $\Delta T_{urban,pixel}$ and $T_{urban,pixel}$ refer to the SUHI intensity and LST value of the urban pixel, respectively, and T_{rural} is the mean LST of all pixels in rural areas.

Based on these ECOSTRESS LST scenes, we were able to generate insights into the spatial details of SUHI variability at various times of the day and night in GUA. We averaged SUHI intensity for the pixels that are cloud free in urban areas to obtain mean SUHI intensity and standard deviation (SD) for each city to examine the diurnal dynamics of city-to-city thermal contrasts in the study area. Afterwards, we also grouped the SUHI values in each city into three levels (i.e., high, moderate, and low) by the regional mean SUHI intensity and SD to evaluate the spatial heterogeneity of SUHI effect risk diurnally from a regional perspective. To this end, we first calculated the mean SUHI value and the corresponding SD of all the urban pixels in GUA for each observation time. The high, moderate, and low levels were then defined as SUHI values that were in the range of $>$ Mean + SD, [Mean, Mean + SD], and $<$ Mean, respectively (Chen et al., 2022; Hua et al., 2021). Following that, we calculated the percentage of pixels at each SUHI level for each city at each observation time.

Finally, we explored the possible driving factors of the inter- and

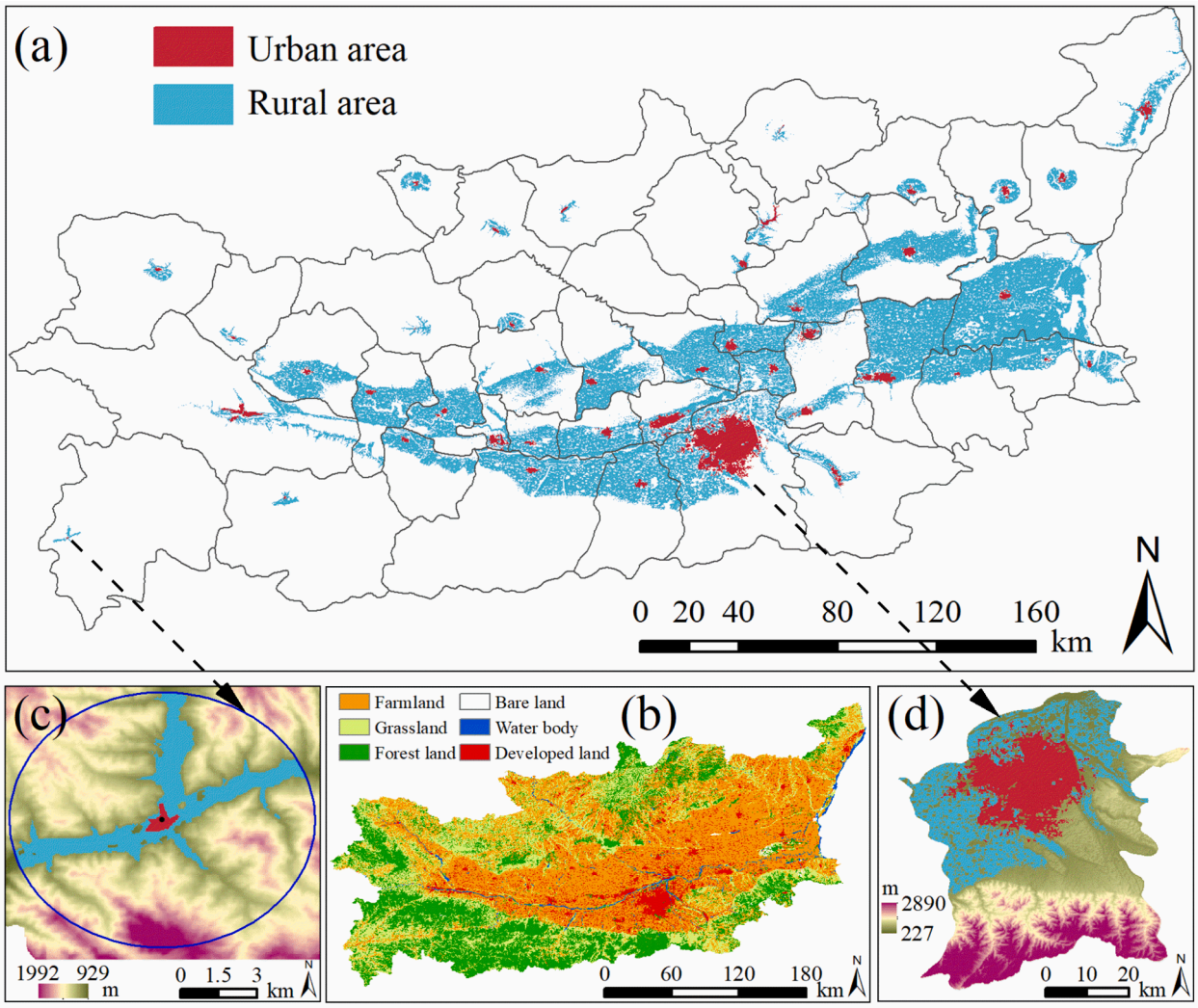

Fig. 3. Delineation of the urban and rural areas for the cities (a), and land cover map of 2020 (b) in the study area. Samples of urban-rural delineation for the city of Fengxian in mountainous areas (c) and Xi'an (d). The elevation map serves as the base map in (c) and (d).

intra-city SUHI variations in GUA and how their impacts varied in the diurnal cycle. Ten factors associated with climatic conditions, land covers, urban features and socioeconomic metrics were used in the analysis. To interpret the SUHI differentiation by city, we initially calculated mean values of air temperature (MAT), wind speed (Wind), precipitation (Prec), urban elevation (UDEM), urban impervious surface percentage (UISP), urban area size (UAS) and population density (PD) for each city. The gross domestic production (GDP) data were directly extracted from the 2020 Shaanxi Statistical Yearbook. Meanwhile, we also quantified the differences in NDVI (ΔNDVI) and solar radiation (ΔSrad) between the urban and the rural pixels as explanatory variables. Before performing such calculations, all these datasets were resampled to match the 30 m land cover data used for the delineation of the urban-rural pixels. Then, we analyzed Pearson's correlations of SUHI intensity with these variables to examine their diurnal controls on SUHI variations among cities in GUA. We further investigated the dominant driving factors accounting for the intra-city SUHI variability at the pixel scale. To comply with the 70 m ECOSTRESS pixel, only NDVI and urban ISP data with 30 m spatial resolution were incorporated in this analysis. We subsequently aggregated the 30 m NDVI and urban ISP data to match the 70 m ECOSTRESS LST data at each observation time and calculated the Pearson's correlation coefficients for each city to measure how urban vegetation and imperviousness influenced the spatial variations of SUHI diurnally. In addition, to provide more direct insight into the impact of land cover on SUHI, we statistically analyzed the mean LST and SD for the main land types across the GUA and for different levels of ISP and NDVI across urban pixels.

3. Results

3.1. ECOSTRESS LST data for SUHI diurnal analysis across the urban agglomeration

Fig. 4 shows the performance of ECOSTRESS, Landsat and ASTER in acquiring LST measurements for the GUA, and thereby providing evidence for the ability of ECOSTRESS LST in fine-grained analysis of SUHI diurnal dynamics over urban agglomerations. ECOSTRESS imagery has a much larger swath width of ~400 km than that of Landsat (~185 km) and ASTER (~60 km) imagery. Such a remarkable advantage enables ECOSTRESS to simultaneously record the fine spatial-resolution LST for multiple cities in an urban agglomeration, generally spanning a broad region. As shown in Fig. 4a, an ECOSTRESS image can provide nearly full coverage of the GUA, while at least three Landsat images and more ASTER images were required to cover the same region. Moreover, these images could be acquired up to several days or nearly two weeks apart, which can make the image merging process even more challenging because of the different acquisition times. In addition, only five Landsat and eight ASTER images with relatively high quality (cloud cover less

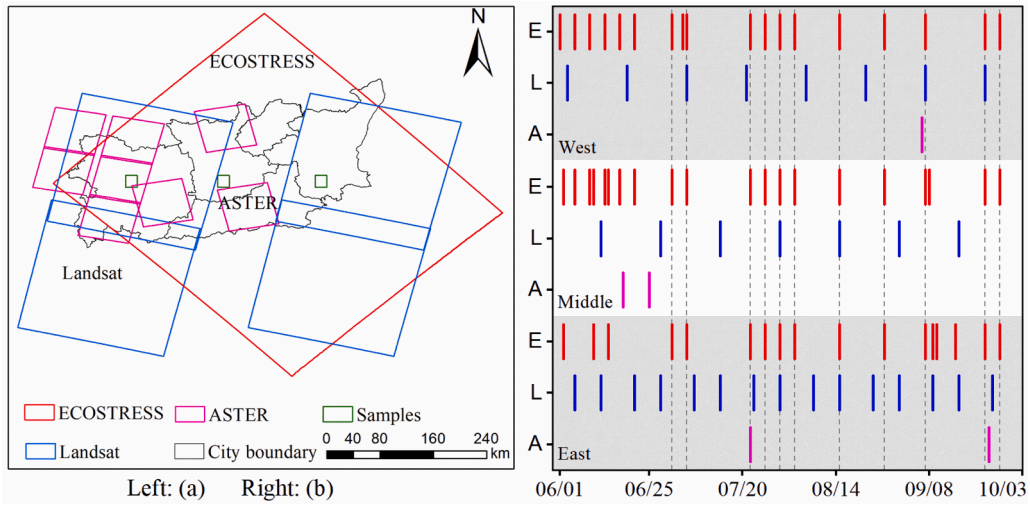

Fig. 4. The spatial extent and distribution of ECOSTRESS (E), Landsat (L) and ASTER (A) LST data across the GUA (a), and data availability (note that we listed all the available images including those with cloud contamination to exhibit their potential to monitor the LST of GUA) in the three sampling areas (b) during the period from June 1, 2020, to September 30, 2020.

than 10%) were available during the period from June to September 2020due to long repeat cycle of Landsat and ASTER and cloud contamination or bad weather conditions. Fig. 4b suggests that the temporal resolution of ECOSTRESS data in each sampling area was much higher than that of Landsat and ASTER data. Furthermore, ECOSTRESS had eleven diurnal LST measurements covering the sampling areas simultaneously, which was impossible for Landsat and ASTER.

Fig. 5 shows the comparison between ECOSTRESS and MODIS in capturing LST magnitude and spatial details over cities of different urban sizes in GUA. Results illustrated that 1 km MODIS LST had clear limitations in elucidating the spatial variability of SUHI in these cities, especially in small cities or cities with long and narrow urban areas (Fig. 5b). For instance, MODIS has weak performance in characterizing LST over the periphery of urban areas. The coarse spatial resolution of MODIS makes it difficult to visually identify the city from the background region. While the ECOSTRESS data can well differentiate the spatial details of LST associated with land cover distribution (Fig. 5c). This is more evident from the pixel-scale LST analysis in urban areas via three pairs of ECOSTRESS and MODIS measurements acquired within short time intervals (Fig. 5d). Apart from that, urban LST data measured by ECOSTRESS and MODIS data also showed a large difference in magnitude. For example, on August 1, 2021, the mean urban LST of FX, DL and BJ quantified by ECOSTRESS and MODIS were 41.9 °C, 48.6 °C and 49.5 °C at 14:13, and 32.3 °C, 41.5 °C and 40.4 °C at 12:42. On August 6, 2022, they were 39.0 °C, 48.5 °C and 47.2 °C at 11:50 measured by ECOSTRESS, and 32.6 °C, 40.3 °C and 40.6 °C at 10:30 measured by MODIS. While on July 26, 2020, they were 30.8 °C, 35.8 °C and 36.8 °C at 16:55 measured by ECOSTRESS, and 31.8 °C, 31.8 °C and 40.1 °C at 13:36 measured by MODIS. The difference in the mean value of urban areas between ECOSTRESS LST and MODIS LST can reach up to about 9 °C. Temporally, such differences may arise from the varying acquisition times of ECOSTRESS and MODIS imagery, despite the short time intervals. Spatially, the inferior performance of 1-km resolution MODIS data in identifying LST over the periphery of urban areas can also contribute to such differences, as shown in Fig. 5b and 5c. In addition, differences in sensor view angles, emissivity determination algorithms and systematic errors may also impact the LST records from MODIS and ECOSTRESS (Botje et al., 2022).

3.2. Characteristics of inter- and intra-city SUHI at varying times of day and night over GUA

Fig. 6 demonstrates the spatial distribution of daytime and nighttime LST at 70 m grid resolution across the study area. Overall, although there was obvious difference in values between LST acquired at different time-stops in the diurnal cycle, their spatial distribution exhibited similar patterns, characterized by distinct, higher LST in urban areas (particularly in the urban area of Xi'an and Xianyang) and lower LST in vegetated areas. In more detail, the spatial pattern of LST in the study area was generally related to the spatial arrangement of different land covers: developed land had the highest LST, followed by farmland, grassland, and forest; the coolest daytime and nighttime LST was more likely to occur in the surrounding mountainous areas, which had not only dense vegetation but also higher elevation. These patterns implied that vegetation tended to cool the surface, while impervious surface tended to warm the surface, and such effects may vary at different times of day and night. Besides, LST in GUA also showed distinctly temporal fluctuations at different times/dates. In general, high LST magnitude and more spatial variations tended to occur around midday, largely due to the heating effect of solar radiance. For instance, at 14:13 on August 1, 2021, the regional LST had a mean value of 38.7 °C and the SD of 7.5 °C (Fig. 6c). Meanwhile, large-scale climatic conditions also affected the temporal variations of regional LST. In Fig. 6e and 6f, the study area possessed a mean LST of 23.2 °C (SD = 5.9 °C) at 16:23, while 30.4 °C (SD = 5.9 °C) at 16:42. Since these scenes were obtained at different times on varying dates, the differences in LST among them were jointly affected by both day-to-day and diurnal variations.

Fig. 7 elucidates the complex characteristics of diurnal SUHI intensity at the city scale in the study area. To facilitate the inter-city SUHI comparison among these observation times, the SUHI values were presented in seven groups at 2 °C intervals. The spatial distribution of cities was provided in Fig. 1 and Appendix Fig. A.1. During the study period, most cities in GUA exhibited positive SUHI intensity, in which the maximum SUHI value could reach up to about 10 °C. Meanwhile, the spatial patterns of SUHI among cities and the SUHI of each individual city varied diurnally. Cities had distinctly higher SUHI at 11:50 and 14:13 than at other observation times. At 11:50, Changwu, a small city, had the highest mean SUHI intensity of 8.3 °C with SD of 2.2 °C, followed by Liquan (SUHI of 7.6 °C, SD of 2.2 °C) and Weinan (SUHI of 7.4 °C, SD of 2.1 °C), while the megacity Xi'an possessed the mean SUHI of 3.7 °C with SD of 3.1 °C, raking 25th among all cities. At 14:13, the most significant SUHI intensity of 10.9 °C with SD of 2.4 °C occurred in the city of Weinan, followed by 10.4 °C with SD of 2.6 °C in the small city of Zhouzhi, and 8.2 °C with SD of 1.7 °C in the small city of Changwu. Xi'an had a relatively low mean SUHI of 5.8 °C with SD of 3.5 °C at this time, ranking 14th among all cities. It can be seen that not only big cities but

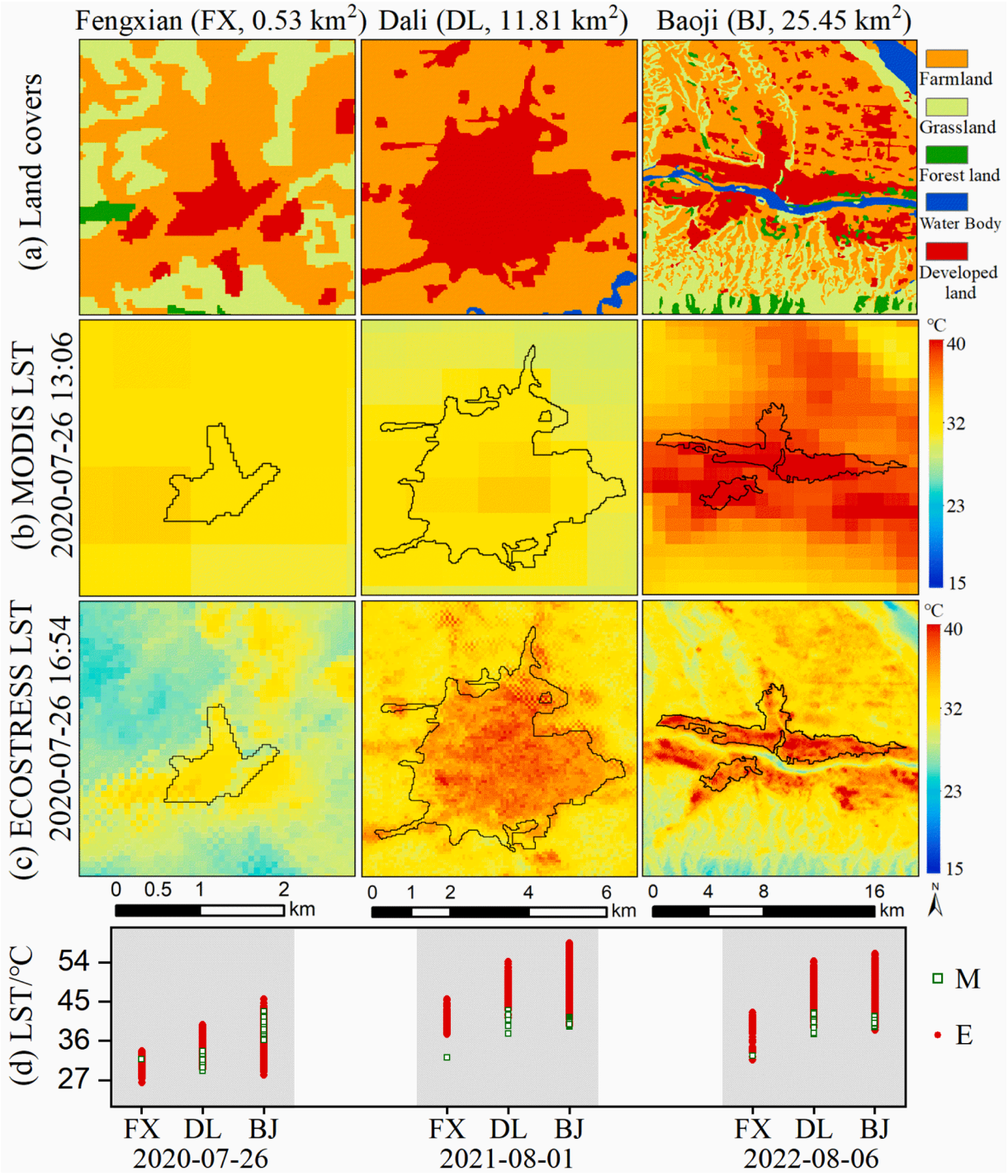

Fig. 5. Comparison of MODIS (1 km spatial resolution) and ECOSTRESS (70 m spatial resolution) data in measuring the spatial details of LST over the cities of different urban sizes in GUA. M and E refer to MODIS and ECOSTRESS, respectively.

also small cities in GUA were exposed to severe SUHI risk. Furthermore, the SUHI values at 14:30, 16:23 and 17:32 were lower than those at the adjacent times. This could be mainly because the collection dates of these three images were all in late September, when the local climate had shifted to cooler autumn. In addition, the mean nighttime SUHI of cities at 23:44, 23:57, 04:25 and 06:59 were 2.0 °C, 3.3 °C, 1.5 °C and 0.9 °C, respectively. At late nighttime or early morning, most cities exhibited lower SUHI with values between 0 °C and 2 °C (Fig. 7k and 7l). However, as shown in Fig. 7j, the nighttime SUHI among the cities in GUA could also be significant at midnight, when most cities had SUHI intensity greater than 2 °C and the maximum SUHI reached 5.2 °C with SD of 1.6 °C in the small city of Qishan.

We further examined the intra-city SUHI variations at the pixel scale to evaluate the diurnal heat exposure and status of each city in GUA (Fig. 8). The full names of these abbreviated cities were presented in Appendix Table A.3. The left and right y-axes presented collection times, and the corresponding regional mean SUHI and SD, respectively. While the x-axis at the bottom represented different cities in the study area. We found that GUA suffered notable SUHI risk at the regional scale, as evidenced by high regionally averaged SUHI around midday and midnight (e.g., 4.2 °C at 11:50, 5.5 °C at 14:13, and 2.6 °C at 23:44). Furthermore, the configurations of the three SUHI levels in most cities

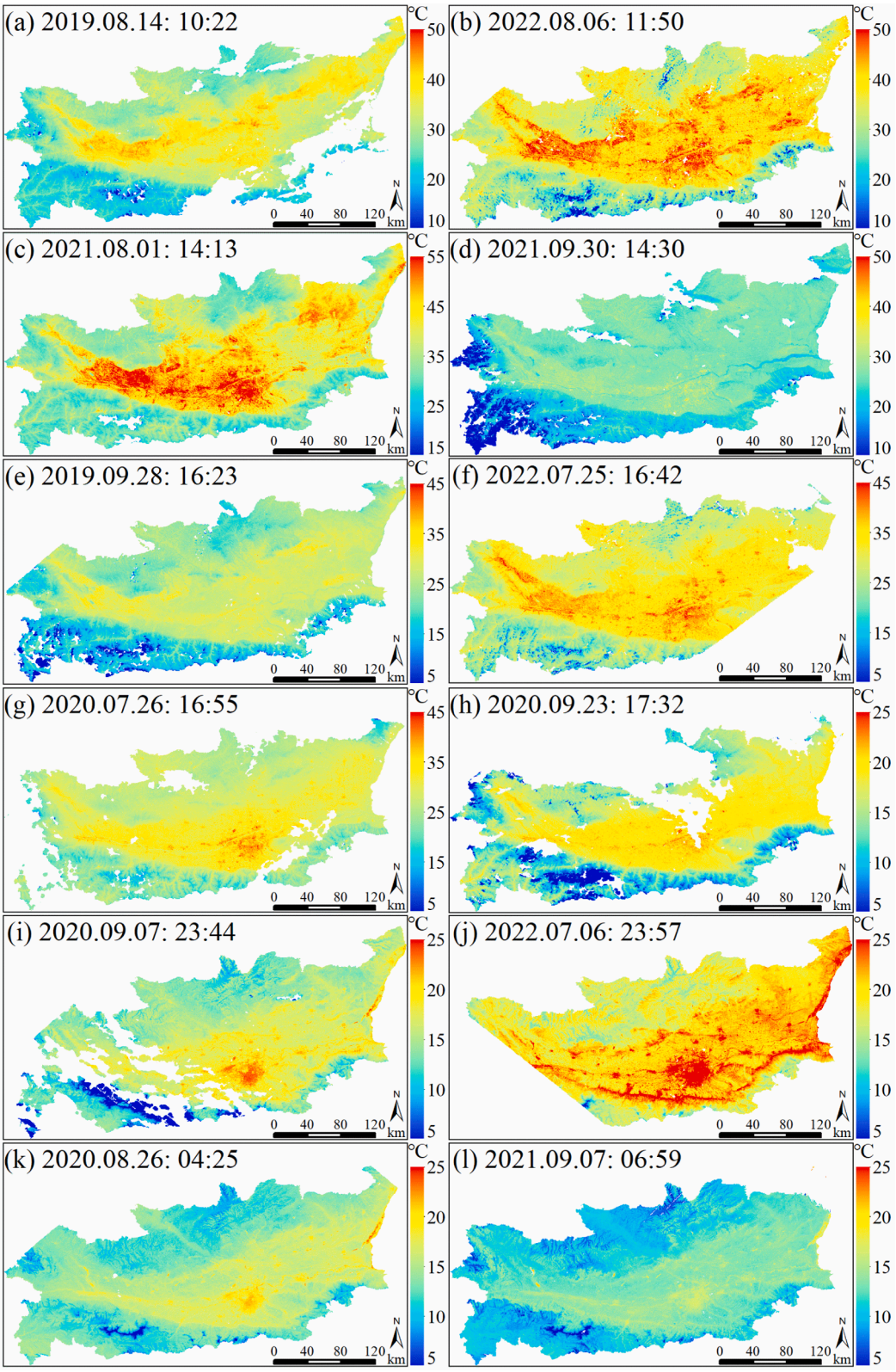

Fig. 6. Distribution of LST across the Guanzhong Urban Agglomeration based on the twelve ECOSTRESS scenes collected from June to September in 2019, 2020, 2021 and 2022. Data are missing for white pixels within the study area. The sequence of LST scenes is arranged by acquisition time in the diurnal cycle.

varied at different times, implying the complex SUHI variability in GUA. For instance, in the county of Liquan (LQ) and Zhouzhi (ZZ), high-level SUHI tended to dominate in the daytime, while in the nighttime SUHI was more likely to be at the low level. In addition, these results together with the urban sizes can provide a comprehensive insight into the thermal condition of each city as well as the contribution of each city to the regional heat stress at different times, which were essential for developing heat mitigation strategies.

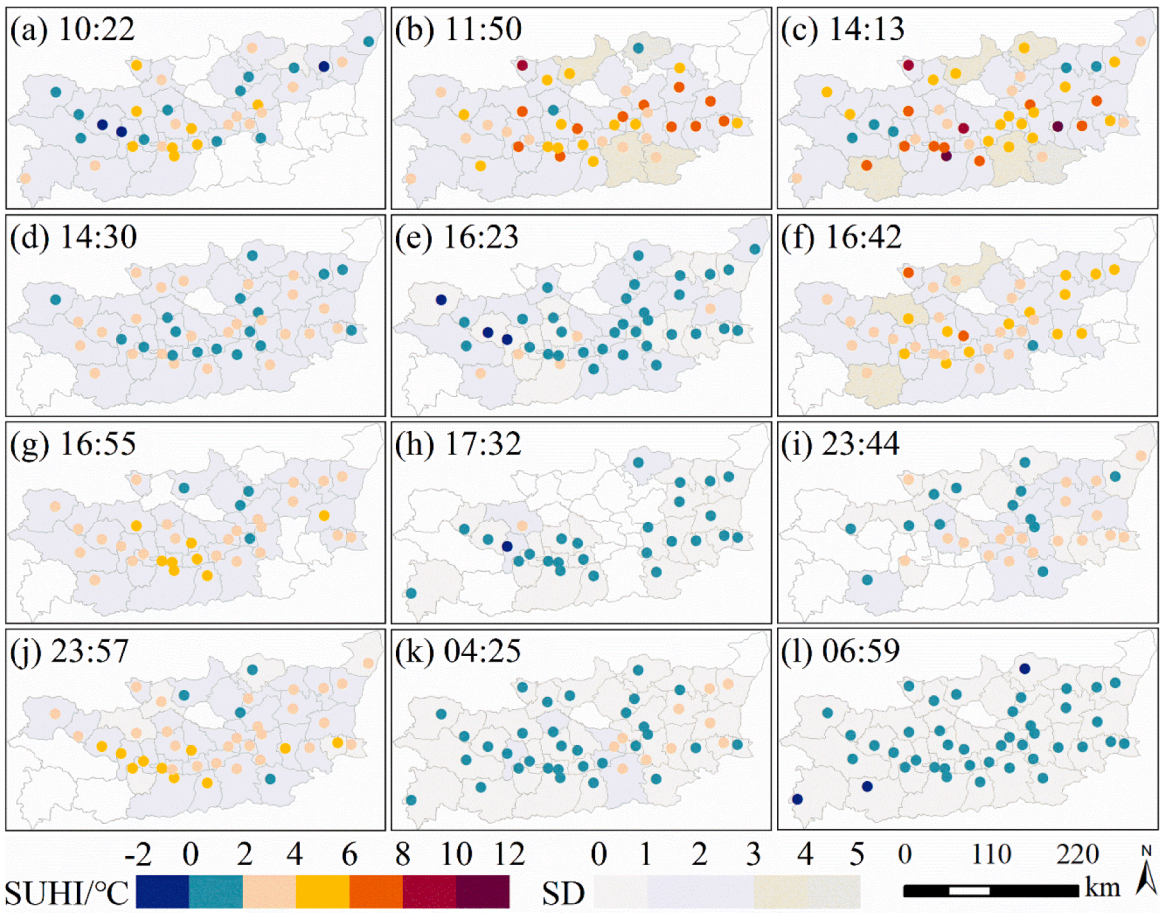

Fig. 7. The spatial patterns of diurnal SUHI intensity in the Guanzhong Urban Agglomeration. White areas refer to cities with missing data. The SUHI intensities were generated only for cities in which both urban and rural areas had over 90% available ECOSTRESS LST pixels.

3.3. Relationship between SUHI and driving factors in the diurnal cycle

Fig. 9 illustrates the correlations of ten variables with variations of SUHI by city at varying diurnal times in GUA. It was clear that the impacts of these factors on SUHI varied diurnally, characterized by stronger correlations at nighttime than at daytime. Vegetation, urban elevation, radiation, precipitation, and wind speed had significant negative influences on nighttime SUHI but had no significant effect on daytime SUHI variations. It is noteworthy that there was a significant negative correlation between urban elevation and nighttime SUHI in the study area, which has received relatively little attention in previous research. This finding indicated that higher altitudes could play an effective role in alleviating the nighttime SUHI in GUA. The insight has important implications for regional urban planning, such as site selection for new urban areas or the direction of urban expansion. Also, urban impervious surface and mean air temperature were positively related to the city-by-city SUHI variations at nighttime, but such influences were less substantial at daytime. Furthermore, urban size, GDP and population density were also not significantly correlated with the inter-city SUHI variations during both daytime and nighttime. Such relationships suggested the complicated integrated effects of these factors on SUHI variations among cities at the regional scale, especially in the daytime with intense and changing incident solar radiation.

ECOSTRESS data with 70-m spatial resolution also allows us to examine how urban vegetation and impervious surface regulate intra-city SUHI variations across GUA in more details (Fig. 10). As expected, both impervious surface and vegetation can partly explain the spatial variations of daytime and nighttime SUHI within each city, with significant positive and strong negative correlations, respectively. Moreover, our results showed that their impacts on the pixel-to-pixel SUHI variations varied across different cities in GUA as well as at different diurnal times in the same city. Taking Xi'an (XA) and the county of Lantian (LA) as examples, we provided insight into the variability of these effects. In Xi'an, the positive impact of urban imperviousness on intra-city SUHI variations was greater at daytime than at nighttime, especially at midday with intense solar radiation. Besides, the correlations between vegetation and intra-city SUHI variations were clearly stronger at daytime than at nighttime. By contrast, in the small city of Lantian, there was stronger correlation between urban imperviousness and intra-city SUHI variations at daytime than at nighttime. Besides, vegetation had higher correlations with intra-city SUHI variations at nighttime than at daytime, implying a more significant cooling effect during the nighttime. Furthermore, according to the correlations map as shown in Fig. 10, such an analysis can be extended to other cities to identify the dominant regulators of daytime and nighttime SUHI to support more effective heat mitigation measures locally.

To generate a more intuitive perspective of land-cover impacts on the regional heat environment, we finally statistically analyzed the thermal features of different surface elements during both daytime and nighttime (Fig. 11). Our results confirmed the warming effect of built-up lands, along with the cooling effect of vegetated elements in GUA. Moreover, we provided specific daytime and nighttime LST differences by land cover type, urban impervious surface, and urban vegetation via spatial analysis at the regional scale. In urban areas, LST increased with the increment of percent impervious surface, which can lead to the mean value differences of 2.9 °C at daytime (Fig. 11c) and 1.8 °C (Fig. 11d) at nighttime. The cooling effect of urban vegetation varied more obviously with vegetation conditions, as evidenced by mean LST differences of 5.5

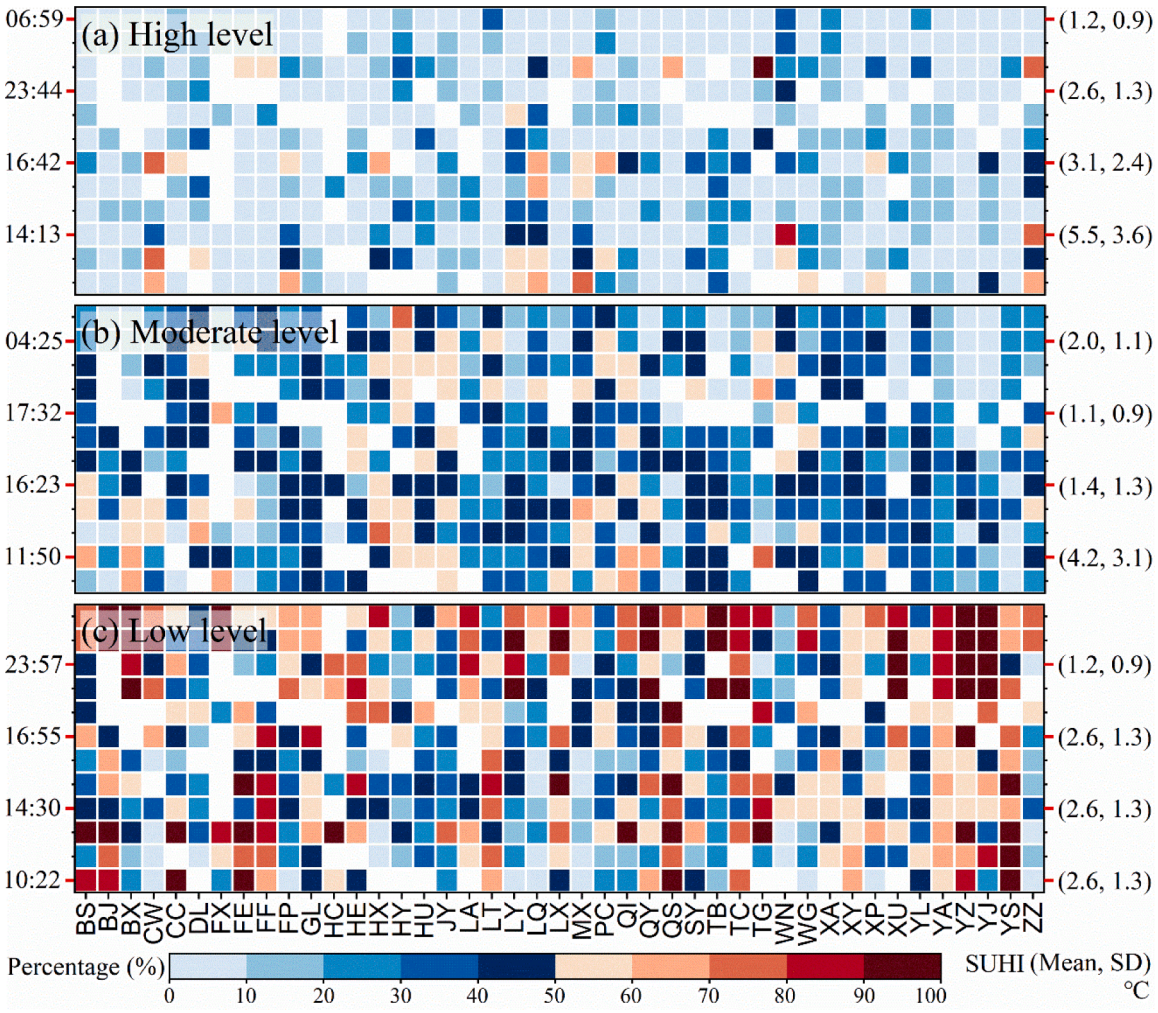

Fig. 8. The percentages of the three SUHI levels in each city at different observation times. The high, moderate, and low level was defined as the SUHI values that were in the range of > Mean + SD, [Mean, Mean + SD], and < Mean, respectively. The Mean and SD refer to the mean SUHI value and corresponding standard deviation of all the urban pixels in GUA at different collection times. Unfilled pixels refer to missing data.

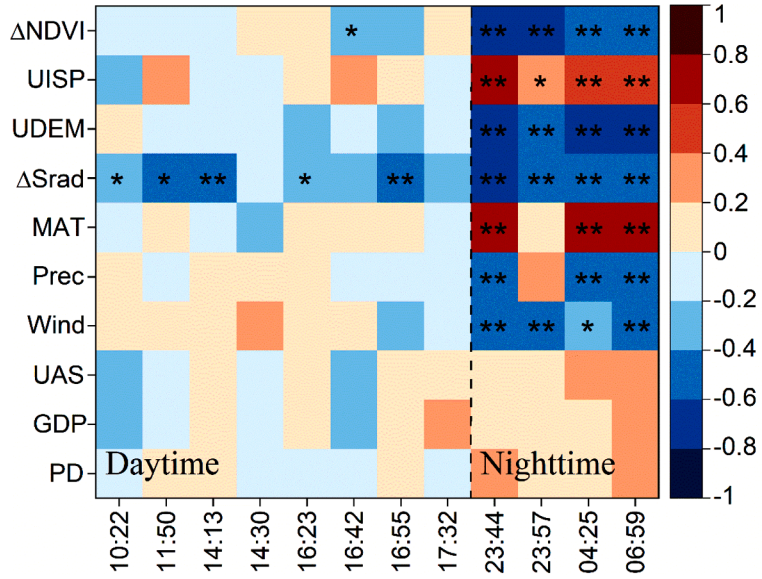

Fig. 9. Relationships between citywide SUHI and the possible driving factors at different observation times in GUA. X-axis indicates collection time points in the diurnal cycle, y-axis indicates different explanatory factors with the format of abbreviation. ** denotes $p < 0.01$ in the significance test. * denotes $p < 0.05$ in the significance test.

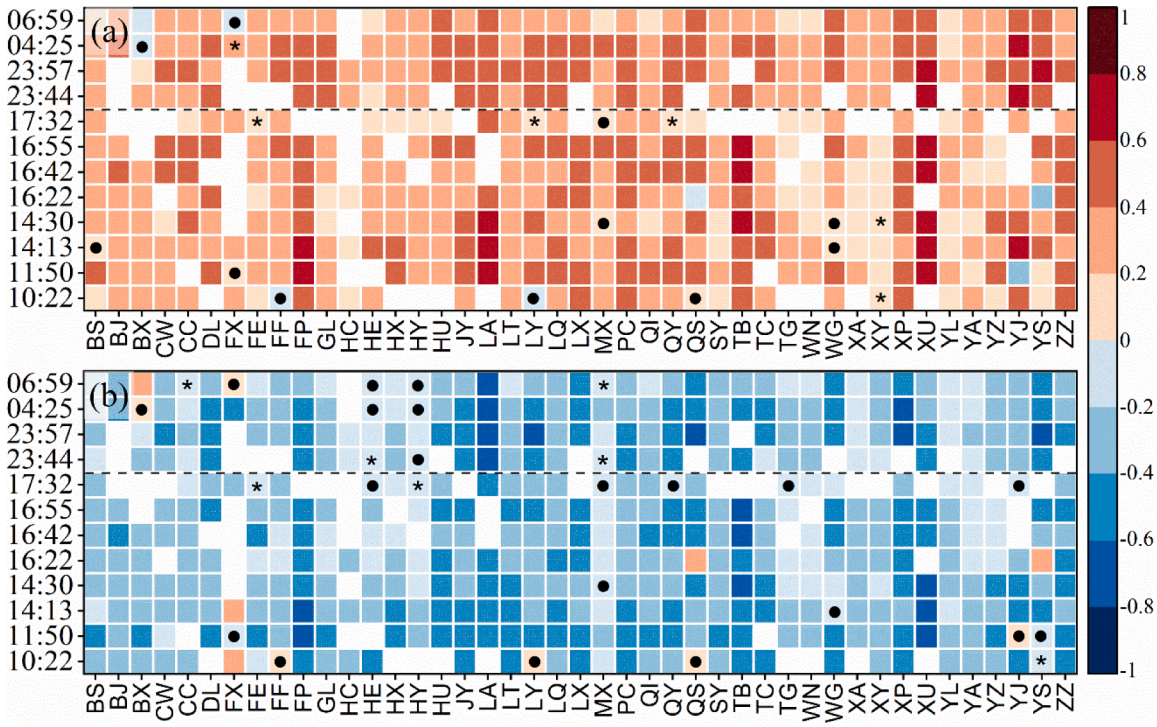

Fig. 10. Correlations of SUHI with UISP (a) and NDVI (b) at pixel scale in each city. The black dot denotes $p > 0.05$ in the significance test. * denotes $p < 0.05$ in the significance test. Note that other unmarked grids all pass the significance test, with $p < 0.01$.

°C at daytime (Fig. 11e) and 2.5 °C at nighttime (Fig. 11f) between dense and sparse vegetation.

4. Discussion

Taking Guanzhong Urban Agglomeration as the study area, this study revealed the fine-grained spatial details of diurnal SUHI patterns and the possible determinants using ECOSTRESS LST data. Our work is the first effort to assess the performance of ECOSTRESS LST in characterizing diurnal SUHI dynamics over urban agglomerations, which is crucial to advance the understanding of urbanization effect on regional thermal environment, as well as to inform the local heat mitigation measures and future urban planning policies.

4.1. Capability of ECOSTRESS data in exploring diurnal variations of SUHI over urban agglomerations

Our results highlight the ability of ECOSTRESS LST in exploring SUHI diurnal dynamics over urban agglomerations that spans broad regions and include cities of various sizes. We provided an effective approach to advance studies of regional SUHI diurnal dynamics by integrating this freely and publicly available new data into scientific research. Such exploration is warranted to meet the imperative need to confront the changing future climate because of the marked regional disparities in the effect of global warming (Sun et al., 2019). Due to the LST data availability, previous studies largely focused on the urban thermal environments in single cities or among some prevalent cities worldwide, yet systematic knowledge of the regional SUHI effect is lacking (Zhou et al., 2022). Considering the advantages (e.g., fine spatial resolution, large imagery size, and more frequent records) of ECOSTRESS along with its global sampling ability, we deem that the proposed procedure of regional SUHI analysis can be extended to other urban agglomerations, especially where more ECOSTRESS samples. Furthermore, compared to the previous studies with the main data sources of MODIS, Landsat and ASTER LST (Wang et al., 2022; Yu et al., 2019), our findings gained a more complete perspective of SUHI patterns at the urban agglomeration level at higher spatial (i.e., encompassed a wide range of city sizes and urban environments) and temporal (i.e., included more time points in the diurnal cycle) scales. In addition, we chose the SUHI investigation to exemplify the enormous potential of ECOSTRESS LST data in regional heat-related research. Our results emphasized that ECOSTRESS can capture the simultaneous LST for large regions more frequently and at a 70 m resolution for varying times of day/night. Since LST is a fundamental parameter for monitoring and modeling Earth surface processes, using ECOSTRESS data as validation data or integrating them into current remote sensing systems can have the potential to optimize relevant model performance (e.g., LST data fusion models, regional climate models, diurnal/annual temperature cycle models) on regional scales (Lai et al., 2018; Wang et al., 2022; Zhang et al., 2022).

4.2. Diurnal variations of SUHI and underlying mechanisms over urban agglomerations

The findings also generated a fresh picture of spatial-detailed SUHI variability diurnally in the Guanzhong Urban Agglomeration. We employed a simplified urban-extent algorithm instead of a buffer-based approach for urban-rural delineations at the administrative scale in GUA, given that it is difficult to determine a fixed buffer to reasonably suit all cities with a wide range of urban sizes and geographic features (Chakraborty & Lee, 2019). Meanwhile, this method exhibited its advantages in fostering the comparability and standardization of SUHI results, as well as in facilitating local policy-making (Chakraborty et al., 2020; Hu et al., 2022). Moreover, through using the updated land cover data with high spatial resolution and providing a scheme for its application in mountainous cities with small urban sizes, our study also reduced the limitations of this method to a certain extent. We then found that the spatial patterns of SUHI among cities, as well as the SUHI of each individual city varied in the diurnal cycle over the GUA. Collectively, inter-city SUHI variations showed higher variability in the late morning, midday, and early afternoon than at evening, midnight and early morning, indicating the unequal exposure of residents to the SUHI

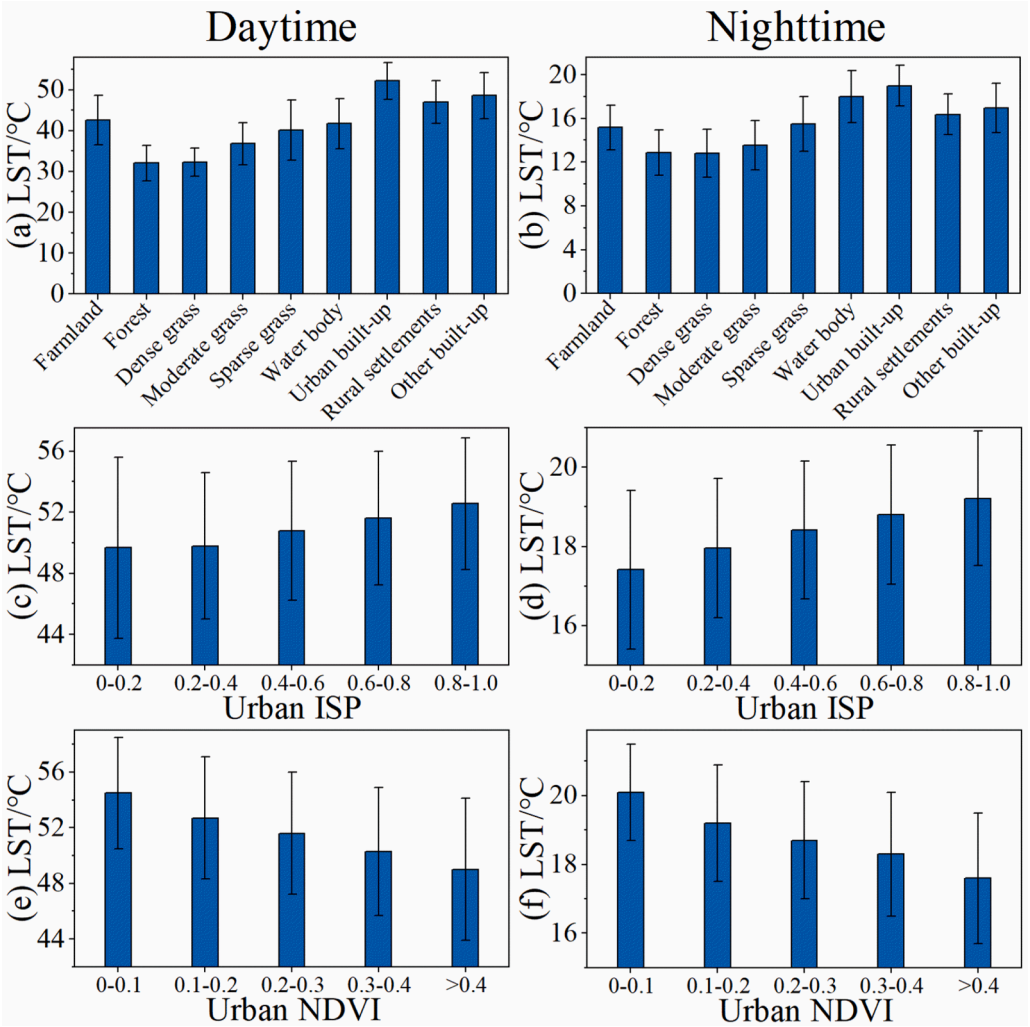

Fig. 11. Mean LST for different land covers, urban impervious surface percentage and urban NDVI at daytime (a), (c), (e), and nighttime (b), (d), (f) based on two selected LST scenes (acquisition times: 14:13 and 04:25).

effect throughout the diurnal cycle. This can be partly explained by the different warming and cooling rates of surface materials/landscapes under varying solar radiation conditions (Krayenhoff et al., 2018). Moreover, our results suggested that not only big cities but also small cities in GUA were exposed to severe SUHI risk. Previous studies were more inclined to analyze SUHI in large-population cities, while pervasively ignoring small cities. However, with low income, inadequate green infrastructure and ongoing urbanization, small cities can be more susceptible to extreme heat. More attention should be paid to the heat stress in small cities, which will benefit a larger portion of the world population (Reba & Seto, 2020). Our evaluation of the intra-city SUHI variations in each city of GUA also provided evidence for nonnegligible urban heat stress in small cities, and thereby can further inform regional heat mitigation measures. According to the results, small cities in GUA, such as the county of Zhouzhi (ZZ), had not only higher mean SUHI intensity but also a larger ratio of high-level SUHI pixels, than Xi'an and the four large cities of GUA, pervasively at different collection times. This can be explained by the high LST of the rural reference areas for these large cities. Furthermore, the weak correlation between the urban size and the SUHI intensity also provides evidence to support this point (Fu et al., 2022; Peng et al., 2012). In addition, compared with the results of previous regional SUHI studies (Sun et al., 2019; Yu et al., 2019; Zhou et al., 2018), our results based on ECOSTRESS LST data documented a more changeable inter- and intra-city SUHI at the regional scale. This is mainly because our study reflected real variations in SUHI intensity over the study area rather than the temporally or spatially averaged results. In many cases (e.g., heat wave duration), practical results may be preferable for assessing the real heat exposure locally, as spatial and temporal aggregation can dilute the SUHI risk intensity and thus hide the nature of the problem (Mentaschi et al., 2022; Ossola et al., 2021; Zuo et al., 2015).

By examining the correlations of SUHI with ten possible driving factors, our results showed their disproportionate contributions to SUHI variations in daytime and nighttime or at inter- and intra-city scales. Background climates and land covers were significantly related to the nighttime SUHI variations among cities in GUA, while these relationships were insignificant during the daytime, which is partly consistent with the earlier findings for other regions (Du et al., 2016; Wang et al., 2018). Moreover, we found that urban elevations had a strong negative effect on nighttime SUHI among cities in GUA. This may be because cities with higher elevation tended to have better ventilation, which can help the heat release at nighttime. Correlation analysis among cities suggested the complex nonlinear effects of these factors on inter-city daytime SUHI at the regional scale. Anthropogenic heat emissions are a significant contributor to urban thermal environment (Feng et al., 2023). A recent study has shown that reduction of human activities due to the COVID-19 lockdown can decrease the daytime SUHI by 0.25 °C and 0.23 °C at nighttime in cold months over megacities (Liu et al., 2022). As the reduction may be smaller in warm months and smaller cities with fewer populations, the impact of COVID-19 lockdown on the

spatial variations of SUHI in GUA cities was not analyzed in this study. Consistent with previous studies, our results also provided evidence for the cooling effect of urban vegetation and the warming effect of urban imperviousness. Concurrently, benefiting from the fine spatial resolution of ECOSTRESS LST, this study further unraveled inter-city disparities in the regulations of urban vegetation and imperviousness on intra-city SUHI. The disparities can partly be attributed to diverse urban landscapes (e.g., 3D structures) and human activities in different cities across GUA. Together with the detailed SUHI characteristics of each city, these correlations can inform more effective and rigorous heat mitigation measures locally. In addition, ECOSTRESS is able to collect nighttime LST measurements at fine spatial resolution (70 m), yet allowing more sufficient examination of daytime and nighttime thermal contrast of land covers (Chang et al., 2022). Our results revealed that the nine land cover types in GUA showed similar thermal patterns at daytime and nighttime despite the significant difference in magnitude. This illustrates the key role of the spatial arrangement and the extent of different land covers in contributing to the spatial LST variations, and thus to the spatial patterns of SUHI.

4.3. Limitations and uncertainties

Our study was devoted to providing a promising scheme for studies toward the diurnal evolution of SUHI for urban agglomerations encompassing diverse urban environments. With the help of ECOSTRESS LST, we generated a more complete perspective of SUHI characteristics in the urban agglomeration at finer spatiotemporal scales, which can certainly reduce the knowledge gap of diurnal SUHI dynamics at the regional scale. However, limitations and uncertainties also existed in our analysis. First, uncertainty may be introduced when employing land cover map for the urban-rural delineation via a simplified urban-extent algorithm. Given that the uncertainty of the land cover map in identifying urban pixels can have impact on the SUHI calculation in cities, especially in small cities. To reduce such uncertainty, we excluded built-up pixels in the reference areas from SUHI analysis in this study. Developing urban change detection algorithms focused on all-sized cities will foster a more accurate examination of regional SUHI variability in space and time. Second, uncertainty can also be introduced due to the influence of cloud. Cloud contaminations are almost inevitable issues when utilizing remotely sensed LST data for SUHI studies at large spatial scales. In this study, we focused our analysis on urban areas with less cloudy pixels to confront this uncertainty. Future advances in cloud detection and removal methods can certainly promote regional climate research. Third, this study elucidated spatial SUHI variability of the study area at a few time points in the diurnal cycle rather than throughout the full diel (or diurnal) cycle. With more ECOSTRESS data to become available in the future, the combination of ECOSTRESS LST data and LST data derived from geostationary satellites, such as GOES-R (Chang et al., 2021) and Himawari-8 (Letu et al., 2020), will likely make it possible to better explore the SUHI diurnal patterns at different timescales for urban agglomerations. Finally, limitations also exist in attribution analysis of the intra-city SUHI variations, primarily arising from coarser spatial resolution of the ancillary data. In this study, we were only able to use two factors (i.e., NDVI and UISP with 30 m spatial resolution) to account for the spatial heterogeneity of SUHI within urban areas. Future availability of more data with high spatiotemporal resolution in urban areas can help formulate a more accurate interpretation of the driving forces of SUHI.

4.4. Implications for sustainable cities

This study has implications for informing the sustainable development of the Guanzhong Urban Agglomeration. First, our results revealed the spatial distributions of LST and SUHI at both daytime and nighttime, highlighting the varying heat stress across cities in GUA. The clearly overheating areas shown in Fig. 6 (e.g., Xi'an and Xianyang) and the cities with severe SUHI risk cities shown in Fig. 7-8 (e.g., Changwu, Weinan and Zhouzhi) may require special attention to reduce heat exposure of local populations. Second, correlation analysis results unraveled the disparities in the regulation of urban vegetation and imperviousness on intra-city SUHI among different cities. Urban planners need to identify the key controlling factor (see Fig. 10), thereby developing targeted heat mitigation measures locally. Finally, we found that LST in daytime rose unevenly with the increase of the impervious surface percentage, as shown in Fig. 11. Specifically, in GUA, the daytime LST differences of varying percentages of impervious surface were 0.1 °C between below 20% and 20%−40%, while 1.0 °C between 20%−40% and 40%−60%. Controlling impervious coverage to a certain level (e.g., below ~40%) may have potential for ameliorating urban thermal environment.

5. Conclusions

With the continued global urbanization, SUHI patterns in urban agglomerations have received increasing attention. In this study, we investigated SUHI diurnal patterns and the possible determinants over differently-sized cities in the GUA, Northwest China, using ECOSTRESS LST measurements. A simplified urban-extent algorithm was employed for urban-rural delineations at the administrative scale to facilitate local policy-making. Then we characterized the inter- and intra-city SUHI variability in the diurnal cycle over the study area. The results showed unequal exposures of differently-sized cities to SUHI effects during the diurnal cycle. Intense SUHI effects were observed not only in big cities but also in small cities, where the maximum SUHI value reached up to about 10 °C. Meanwhile, inter-city SUHI showed higher spatial variability in the late morning, midday, and early afternoon than at evening, midnight, and early morning. Our results suggested the notable SUHI risk at the regional scale, as evidenced by high regionally averaged SUHI around midday and midnight (e.g., 4.2 °C at 11:50, 5.5 °C at 14:13, and 2.6 °C at 23:44). The pixel-scale analysis also demonstrated that the thermal condition of each city as well as the contribution of each city to the regional heat stress varied with different diurnal times. In addition, the results showed the disproportionate contributions of background climate, vegetation, urban imperviousness, and elevation to SUHI variations at daytime and nighttime or at inter- and intra-city scales. These factors tended to have significant controls on nighttime SUHI variations among cities in GUA, while such controls were less substantial at daytime. This study further unraveled inter-city disparities in the regulations of urban vegetation and imperviousness on intra-city SUHI. The results demonstrated that their impacts on the pixel-by-pixel SUHI variations varied across different cities in GUA as well as at different diurnal times in the same city.

This study highlights the ability of ECOSTRESS LST in fine-spatial analysis of SUHI diurnal dynamics over urban agglomerations and develops an effective approach for regional SUHI and urban climate studies, which can be extended to other urban agglomerations, as more ECOSTRESS data become available in the future. The results of this study provide a more detailed perspective of SUHI characteristics in the urban agglomeration at higher spatial (i.e., encompassed a wide range of city sizes and urban environments) and temporal (i.e., included more time points in the diurnal cycle) scales, which help advance our understanding of the less-investigated SUHI diurnal dynamics in regions. Our findings focused on administration units can inform more practicable heat mitigation measures locally, and support future regional urban planning policies. Further regional SUHI studies under disparate climate backgrounds and different stages of urbanization can help us better confront the warming future. Finally, we suggest that more attention needs to be paid to SUHI risk issues in small cities.

Declaration of Competing Interest

We declare that we have no known competing financial interests or

personal relationships that could have appeared to influence the work reported in this paper.

Data availability

Data will be made available on request.

Acknowledgments

We acknowledge the support of the Global STEM Professorship by the Hong Kong SAR Government and the financial support of the Hong Kong Polytechnic University through the University Financial Support for Awardees of Major Renowned Funding and Award Schemes. We thank Dr. G. C. Hulley and other members of the ECOSTRESS science team for the development of the ECOSTRESS LST data and the seven anonymous reviewers for their constructive and insightful comments on our manuscript.

Supplementary materials

Supplementary material associated with this article can be found, in the online version, at doi:10.1016/j.scs.2023.104833.

References

Batten, D. F. (1995). Network cities: Creative urban agglomerations for the 21st century. *Urban Studies, 32*, 313–327.

Botje, D., Dewan, A., & Chakraborty, T. C. (2022). Comparing coarse-resolution land surface temperature products over Western Australia. *Remote Sensing, 14*(10), 2296.

Chakraborty, T., Hsu, A., Manya, D., & Sheriff, G. (2020). A spatially explicit surface urban heat island database for the United States: Characterization, uncertainties, and possible applications. *ISPRS Journal of Photogrammetry and Remote Sensing, 168*, 74–88.

Chakraborty, T., & Lee, X. (2019). A simplified urban-extent algorithm to characterize surface urban heat islands on a global scale and examine vegetation control on their spatiotemporal variability. *International Journal of Applied Earth Observation and Geoinformation, 74*, 269–280.

Chang, Y., Xiao, J., Li, X., Frolking, S., Zhou, D., Schneider, A., et al. (2021). Exploring diurnal cycles of surface urban heat island intensity in Boston with land surface temperature data derived from GOES-R geostationary satellites. *Science of The Total Environment, 763*, Article 144224.

Chang, Y., Xiao, J., Li, X., Middel, A., Zhang, Y., Gu, Z., et al. (2021). Exploring diurnal thermal variations in urban local climate zones with ECOSTRESS land surface temperature data. *Remote Sensing of Environment*, 263.

Chang, Y., Xiao, J., Li, X., Zhou, D., & Wu, Y. (2022). Combining GOES-R and ECOSTRESS land surface temperature data to investigate diurnal variations of surface urban heat island. *Science of The Total Environment*, Article 153652.

Chen, Y., Yang, J., Yang, R., Xiao, X., & Xia, J. C. (2022). Contribution of urban functional zones to the spatial distribution of urban thermal environment. *Building and Environment, 216*, Article 109000.

Du, H., Wang, D., Wang, Y., Zhao, X., Qin, F., Jiang, H., et al. (2016). Influences of land cover types, meteorological conditions, anthropogenic heat and urban area on surface urban heat island in the Yangtze River Delta Urban Agglomeration. *Science of The Total Environment, 571*, 461–470.

Fang, C., & Yu, D. (2017). Urban agglomeration: An evolving concept of an emerging phenomenon. *Landscape and Urban Planning, 162*, 126–136.

Feng, R., Wang, F., Wang, K., Wang, H., & Li, L. (2021). Urban ecological land and natural-anthropogenic environment interactively drive surface urban heat island: An urban agglomeration-level study in China. *Environment International*, 157.

Feng, Z., Wang, X., Yuan, J., Zhang, Y., & Yu, M. (2023). Changes in air pollution, land surface temperature, and urban heat islands during the COVID-19 lockdown in three Chinese urban agglomerations. *Science of The Total Environment*, Article 164496.

Fick, S. E., & Hijmans, R. J. (2017). WorldClim 2: New 1-km spatial resolution climate surfaces for global land areas. *International Journal of Climatology, 37*, 4302–4315.

Fu, X., Yao, L., Xu, W., Wang, Y., & Sun, S. (2022). Exploring the multitemporal surface urban heat island effect and its driving relation in the Beijing-Tianjin-Hebei urban agglomeration. *Applied Geography*, 144.

Geng, S., Yang, L., Sun, Z., Wang, Z., Qian, J., Jiang, C., et al. (2021). Spatiotemporal patterns and driving forces of remotely sensed urban agglomeration heat islands in South China. *Science of The Total Environment*, 800.

Guo, J., Huang, G., Wang, X., Wu, Y., Li, Y., Zheng, R., et al. (2020). Evaluating the added values of regional climate modeling over China at different resolutions. *Science of The Total Environment, 718*, Article 137350.

Gustine, R. N., Lee, C. M., Halverson, G. H., Acuna, S. C., Cawse-Nicholson, K. A., Hulley, G. C., et al. (2022). Using ECOSTRESS to observe and model diurnal variability in water temperature conditions in the San Francisco estuary. *IEEE Transactions on geoscience and remote sensing, 60*, 1–10.

Hook, S. J., Cawse-Nicholson, K., Barsi, J., Radocinski, R., Hulley, G. C., Johnson, W. R., et al. (2020). In-Flight Validation of the ECOSTRESS, Landsats 7 and 8 thermal infrared spectral channels using the lake tahoe CA/NV and Salton Sea CA Automated Validation Sites. *IEEE Transactions on geoscience and remote sensing, 58*, 1294–1302.

Hook, S. J., Vaughan, R. G., Tonooka, H., & Schladow, S. G. (2007). Absolute radiometric in-flight validation of mid infrared and thermal infrared data from ASTER and MODIS on the Terra spacecraft using the Lake Tahoe, CA/NV, USA, automated validation site. *IEEE Transactions on Geoscience and Remote Sensing, 45*(6), 1798–1807.

Hou, H., Su, H., Yao, C., & Wang, Z. H. (2023). Spatiotemporal patterns of the impact of surface roughness and morphology on urban heat island. *Sustainable Cities and Society, 92*, Article 104513.

Hu, D., Meng, Q., Zhang, L., & Zhang, Y. (2020). Spatial quantitative analysis of the potential driving factors of land surface temperature in different "Centers" of polycentric cities: A case study in Tianjin. *China. Science of The Total Environment, 706*, Article 135244.

Hu, J., Yang, Y., Zhou, Y., Zhang, T., Ma, Z., & Meng, X. (2022). Spatial patterns and temporal variations of footprint and intensity of surface urban heat island in 141 China cities. *Sustainable Cities and Society, 77*, Article 103585.

Hua, J., Zhang, X., Ren, C., Shi, Y., & Lee, T. C. (2021). Spatiotemporal assessment of extreme heat risk for high-density cities: A case study of Hong Kong from 2006 to 2016. *Sustainable cities and society, 64*, Article 102507.

Hulley, G., Shivers, S., Wetherley, E., & Cudd, R. (2019). New ECOSTRESS and MODIS land surface temperature data reveal fine-scale heat vulnerability in cities: A case study for Los Angeles County, California. *Remote Sensing, 11*(18), 2136.

Hulley, G. C., Göttsche, F. M., Rivera, G., Hook, S. J., Freepartner, R. J., Martin, M. A., et al. (2021). Validation and quality assessment of the ECOSTRESS level-2 land surface temperature and emissivity product. *IEEE Transactions on geoscience and remote sensing*.

Kim, S. W., & Brown, R. D. (2021). Urban heat island (UHI) variations within a city boundary: A systematic literature review. *Renewable and Sustainable Energy Reviews*, 148.

Krayenhoff, E. S., Moustaoui, M., Broadbent, A. M., Gupta, V., & Georgescu, M. (2018). Diurnal interaction between urban expansion, climate change and adaptation in US cities. *Nature Climate Change, 8*, 1097–1103.

Kuang, W., Zhang, S., Li, X., & Lu, D. (2021). A 30 m resolution dataset of China's urban impervious surface area and green space, 2000–2018. *Earth System Science Data, 13*, 63–82.

Lai, J., Zhan, W., Huang, F., Voogt, J., Bechtel, B., Allen, M., et al. (2018). Identification of typical diurnal patterns for clear-sky climatology of surface urban heat islands. *Remote Sensing of Environment, 217*, 203–220.

Letu, H., Yang, K., Nakajima, T. Y., Ishimoto, H., Nagao, T. M., Riedi, J., et al. (2020). High-resolution retrieval of cloud microphysical properties and surface solar radiation using Himawari-8/AHI next-generation geostationary satellite. *Remote Sensing of Environment*, 239.

Liu, J., Liu, M., Tian, H., Zhuang, D., Zhang, Z., Zhang, W., et al. (2005). Spatial and temporal patterns of China's cropland during 1990–2000: An analysis based on Landsat TM data. *Remote Sensing of Environment, 98*, 442–456.

Liu, Z., Lai, J., Zhan, W., Bechtel, B., Voogt, J., Quan, J., et al. (2022). Urban heat islands significantly reduced by COVID-19 lockdown. *Geophysical Research Letters*, 49.

Liu, Z., Zhan, W., Lai, J., Bechtel, B., Lee, X., Hong, F., et al. (2022). Taxonomy of seasonal and diurnal clear-sky climatology of surface urban heat island dynamics across global cities. *ISPRS Journal of Photogrammetry and Remote Sensing, 187*, 14–33.

Mentaschi, L., Duveiller, G., Zulian, G., Corbane, C., Pesaresi, M., Maes, J., et al. (2022). Global long-term mapping of surface temperature shows intensified intra-city urban heat island extremes. *Global Environmental Change*, 72.

Ossola, A., Jenerette, G. D., McGrath, A., Chow, W., Hughes, L., & Leishman, M. R. (2021). Small vegetated patches greatly reduce urban surface temperature during a summer heatwave in Adelaide. *Australia. Landscape and Urban Planning, 209*, Article 104046.

Peel, M. C., Finlayson, B. L., & McMahon, T. A. (2007). Updated world map of the Köppen-Geiger climate classification. *Hydrology and earth system sciences, 11*(5), 1633–1644.

Peng, S., Ding, Y., Liu, W., & Li, Z. (2019). 1km monthly temperature and precipitation dataset for China from 1901 to 2017. *Earth System Science Data, 11*(4), 1931–1946.

Peng, S., Piao, S., Ciais, P., Friedlingstein, P., Ottle, C., Bréon, F. M., et al. (2012). Surface urban heat island across 419 global big cities. *Environmental science & technology, 46*(2), 696–703.

Peng, X., Zhou, Y., Fu, X., & Xu, J. (2022). Study on the spatial-temporal pattern and evolution of surface urban heat island in 180 shrinking cities in China. *Sustainable Cities and Society, 84*, Article 104018.

Reba, M., & Seto, K. C. (2020). A systematic review and assessment of algorithms to detect, characterize, and monitor urban land change. *Remote Sensing of Environment*, 242.

Rigden, A. J., & Li, D. (2017). Attribution of surface temperature anomalies induced by land use and land cover changes. *Geophysical Research Letters, 44*, 6814–6822.

Siddiqui, A., Kushwaha, G., Nikam, B., Srivastav, S. K., Shelar, A., & Kumar, P. (2021). Analysing the day/night seasonal and annual changes and trends in land surface temperature and surface urban heat island intensity (SUHII) for Indian cities. *Sustainable Cities and Society, 75*, Article 103374.

Sims, K., Reith, A., Bright, E., McKee, J., & Rose, A. (2022). *LandScan global 2021*. Oak Ridge, TN: Oak Ridge National Laboratory.

Sun, Q., Miao, C., Hanel, M., Borthwick, A. G. L., Duan, Q., Ji, D., et al. (2019). Global heat stress on health, wildfires, and agricultural crops under different levels of climate warming. *Environment International, 128*, 125–136.

Sun, Y., Gao, C., Li, J., Wang, R., & Liu, J. (2019). Evaluating urban heat island intensity and its associated determinants of towns and cities continuum in the Yangtze River Delta Urban Agglomerations. *Sustainable Cities and Society*, 50.

Voogt, J. A., & Oke, T. R. (2003). Thermal remote sensing of urban climates. *Remote Sensing of Environment, 86*, 370–384.

Wan, Z. (2008). New refinements and validation of the MODIS land-surface temperature/emissivity products. *Remote Sensing of Environment, 112*, 59–74.

Wang, J., Xue, P., Pringle, W., Yang, Z., & Qian, Y. (2022). Impacts of lake surface temperature on the summer climate over the great lakes region. *Journal of Geophysical Research: Atmospheres*, Article e2021JD036231.

Wang, Y., Du, H., Xu, Y., Lu, D., Wang, X., & Guo, Z. (2018). Temporal and spatial variation relationship and influence factors on surface urban heat island and ozone pollution in the Yangtze River Delta. *China. Science of The Total Environment, 631-632*, 921–933.

Wang, Y., Yao, Y., Chen, S., Ni, Z., & Xia, B. (2022). Spatiotemporal evolution of urban development and surface urban heat island in Guangdong-Hong Kong-Macau greater bay area of China from 2013 to 2019. *Resources, Conservation and Recycling*, 179.

Weng, Q. (2009). Thermal infrared remote sensing for urban climate and environmental studies: Methods, applications, and trends. *ISPRS Journal of Photogrammetry and Remote Sensing, 64*, 335–344.

Weng, Q., Fu, P., & Gao, F. (2014). Generating daily land surface temperature at Landsat resolution by fusing Landsat and MODIS data. *Remote Sensing of Environment, 145*, 55–67.

Weng, Q., Rajasekar, U., & Hu, X. (2011). Modeling urban heat islands and their relationship with impervious surface and vegetation abundance by using ASTER images. *IEEE Transactions on geoscience and remote sensing, 49*, 4080–4089.

Xiao, J., Fisher, J. B., Hashimoto, H., Ichii, K., & Parazoo, N. C. (2021). Emerging satellite observations for diurnal cycling of ecosystem processes. *Nature Plants, 7*, 877–887.

Yang, J., Dong, J., Xiao, X., Dai, J., Wu, C., Xia, J., et al. (2019). Divergent shifts in peak photosynthesis timing of temperate and alpine grasslands in China. *Remote Sensing of Environment*, 233.

Yang, Y., Li, Y., & Guo, Y. (2022). Impact of the differences in carbon footprint driving factors on carbon emission reduction of urban agglomerations given SDGs: A case study of the Guanzhong in China. *Sustainable Cities and Society, 85*, Article 104024.

Yang, Y., Zheng, Z., Yim, S. Y. L., Roth, M., Ren, G., Gao, Z., et al. (2020). PM2.5 pollution modulates wintertime urban heat island intensity in the Beijing-Tianjin-Hebei Megalopolis, China. *Geophysical Research Letters*, 47.

Yao, R., Wang, L., Huang, X., Cao, Q., Wei, J., He, P., et al. (2023). Global seamless and high-resolution temperature dataset (GSHTD), 2001–2020. *Remote Sensing of Environment, 286*, Article 113422.

Yu, Z., Yao, Y., Yang, G., Wang, X., & Vejre, H. (2019). Spatiotemporal patterns and characteristics of remotely sensed region heat islands during the rapid urbanization (1995-2015) of Southern China. *Science of the Total Environment, 674*, 242–254.

Zhang, X., Chen, W., Chen, Z., Yang, F., Meng, C., Gou, P., et al. (2022). Construction of cloud-free MODIS-like land surface temperatures coupled with a regional weather research and forecasting (WRF) model. *Atmospheric Environment*, 283.

Zhang, Z., Wang, X., Zhao, X., Liu, B., Yi, L., Zuo, L., et al. (2014). A 2010 update of National Land Use/Cover Database of China at 1:100000 scale using medium spatial resolution satellite images. *Remote Sensing of Environment, 149*, 142–154.

Zheng, Q., Weng, Q., & Wang, K. (2021). Characterizing urban land changes of 30 global megacities using nighttime light time series stacks. *ISPRS Journal of Photogrammetry and Remote Sensing, 173*, 10–23.

Zhou, D., Bonafoni, S., Zhang, L., & Wang, R. (2018). Remote sensing of the urban heat island effect in a highly populated urban agglomeration area in East China. *Science of The Total Environment, 628-629*, 415–429.

Zhou, D., Xiao, J., Bonafoni, S., Berger, C., Deilami, K., Zhou, Y., et al. (2019). Satellite Remote Sensing of Surface Urban Heat Islands: Progress, Challenges, and Perspectives. *Remote Sensing, 11*(1), 48.

Zhou, D., Xiao, J., Frolking, S., Zhang, L., & Zhou, G. (2022). Urbanization contributes little to global warming but substantially intensifies local and regional land surface warming. *Earth's Future*, 10.

Zhu, Z., Zhou, Y., Seto, K. C., Stokes, E. C., Deng, C., Pickett, S. T. A., et al. (2019). Understanding an urbanizing planet: Strategic directions for remote sensing. *Remote Sensing of Environment, 228*, 164–182.

Zuo, J., Pullen, S., Palmer, J., Bennetts, H., Chileshe, N., & Ma, T. (2015). Impacts of heat waves and corresponding measures: A review. *Journal of Cleaner Production, 92*, 1–12.